

Structural, optical, and photoluminescent properties of sol–gel derived Eu-doped Ba_{1–x}Sr_xTiO₃ thin films

Ling Liu · Ni Qin · Dinghua Bao

Received: 10 December 2014 / Accepted: 15 February 2015 / Published online: 22 February 2015
© Springer Science+Business Media New York 2015

Abstract Eu-doped Ba_{1–x}Sr_xTiO₃ ($x = 0, 0.2, 0.3,$ and 0.4) thin films with Eu-doping content of 1 mol% have been prepared on fused silica substrates by a chemical solution deposition method and characterized by X-ray diffraction (XRD), atomic force microscopy (AFM), optical and photoluminescence measurements. XRD analysis showed that the films were well crystallized with a pure perovskite structure in the annealing temperature range from 650 to 750 °C. AFM observation indicated that the films were dense and smooth. The band-gap energies of the thin films were also investigated. The more the Sr content in the thin films, the narrower the energy gap of the thin films. Photoluminescence spectra of the thin films showed two prominent transitions of Eu³⁺ ions at 594 nm (⁵D₀ → ⁷F₁) and 618 nm (⁵D₀ → ⁷F₂) upon excitation at 395 nm (⁷F₀ → ⁵L₆). The observed changes of luminescence spectra by the decrease of the intensity ratio R, which was defined as the ratio of the integrated emission intensity of ⁵D₀ → ⁷F₂ transition to that of ⁵D₀ → ⁷F₁ transition, were associated with the increase of the inversion symmetry of Eu³⁺ sites when Sr content increased. Lifetime study of photoluminescence indicated that the average lifetime of the thin films was approximately 0.7 ms.

1 Introduction

Perovskite-type compounds such as BaTiO₃, SrTiO₃, CaTiO₃, and their solid solution have drawn a great deal of attention due to their attractive ferroelectric and electro-optic properties. Ba_{1–x}Sr_xTiO₃ (BST) is a continuous solid solution between BaTiO₃ and SrTiO₃ over a whole concentration range. The partial replacement of barium by strontium can improve dielectric constant, lower dielectric loss, and increase pyroelectric coefficient. The Curie temperature of BST decreases linearly with increasing Sr concentration. Hence, the electrical and optical properties of BST can be tailored over a broad range to meet the requirements of various device applications [1–3].

Trivalent rare earth ions are commonly doped at a low doping level into BaTiO₃-based materials to further improve material performance. Saha and Krupanidhi reported that La-doped BST thin films showed a large decrease of leakage current in comparison with undoped BST films [4]. Er-doping was confirmed to improve the dielectric property of BST by Shen and coworkers, meanwhile, the up-conversion photoluminescence was also observed [2]. Among all the rare earth ions, trivalent europium (Eu³⁺) ion is well known for acting not only as an activator in many hosts for producing red-light emission, but also as a structural probe, which can be used to investigate the local environment of the cations in the materials, since the luminescence properties of Eu³⁺ are strongly influenced by the local environment around the lanthanide ions [5–8].

Although extensive studies have been done on doped and undoped BaTiO₃-based nanocrystals [5, 9, 10], thin films [1, 11–14], powders [2, 15], and ceramics [16, 17], Eu³⁺-doped BST thin films have not been investigated thoroughly. In this paper, we report the structural, optical, and photoluminescent properties of sol–gel derived

L. Liu · N. Qin · D. Bao (✉)
State Key Laboratory of Optoelectronic Materials and Technologies, School of Physics and Engineering, Sun Yat-Sen University, Guangzhou 510275, China
e-mail: stsbhd@mail.sysu.edu.cn

$\text{Ba}_{1-x}\text{Sr}_x\text{TiO}_3:\text{Eu}$ (BSTE) thin films. Considering that at room temperature, the dielectric constant and tunability of BST thin films were relatively high when Sr content x was <0.4 but started to decrease rapidly as x increased [18], in our study, the Sr content x was chosen at 0, 0.2, 0.3, and 0.4. In addition, the concentration of Eu dopant was kept at 1 mol%. It is a relatively low doping concentration in order to ensure that europium is incorporated into BST host, since the solubility limit of europium in BaTiO_3 host was reported previously to be close to 4 mol% [9, 19].

2 Experimental procedure

The $\text{Ba}_{1-x}\text{Sr}_x\text{TiO}_3:\text{Eu}$ thin films (BSTE, $x = 0, 0.2, 0.3,$ and 0.4) with Eu-doping content of 1 mol% were fabricated by a chemical solution deposition method. We synthesized the precursor solutions using barium acetate, strontium acetate hemihydrate, europium nitrate hexahydrate, and tetrabutyl titanate as starting materials, acetic acid and 2-methoxyethanol as solvent and acetylacetonate as stabilizing reagent. BSTE thin films were prepared on fused silica substrates by spin-coating the precursor solutions at a rotating speed of 3000 rpm for 30 s, and then the thin coating layer was directly put into a furnace whose temperature was set at 550–800 °C to anneal for 5 min. The spin-coating and rapid thermal annealing process was repeated for different times in order to obtain desired film thickness. Finally, the deposited films were annealed at 550–800 °C in air for 2 h and then cooled to room temperature.

The crystal structure of all the samples was analyzed by an X-ray diffractometer (D/MAX 2200 VPC, Rigaku, Tokyo, Japan) with Cu $K\alpha$ radiation operated at a working current of 26 mA and a working voltage of 40 kV. The surface morphology and microstructure of the films were characterized by an atomic force microscopy (Dimension FastScan, Bruker, Germany) using a tapping mode. The photoluminescence spectra were obtained with a spectrofluorophotometer (FLSP920, Edinburgh Instruments, Livingston, UK) equipped with a 450 W Xe900 lamp, and a 60 W $\mu\text{F}900$ lamp as excitation sources and a RP928 red sensitive detector. The UV–Vis spectra were recorded with a spectrophotometer (UV-3150, Shimadzu, Japan).

3 Results and discussion

Figure 1a shows the XRD patterns of the $\text{BaTiO}_3:\text{Eu}$ (BTE) thin films deposited on fused silica substrates annealed at different temperatures. The thin film annealed at 550 °C exhibited an amorphous characteristic, as no obvious diffraction peaks were detected. The broad peak

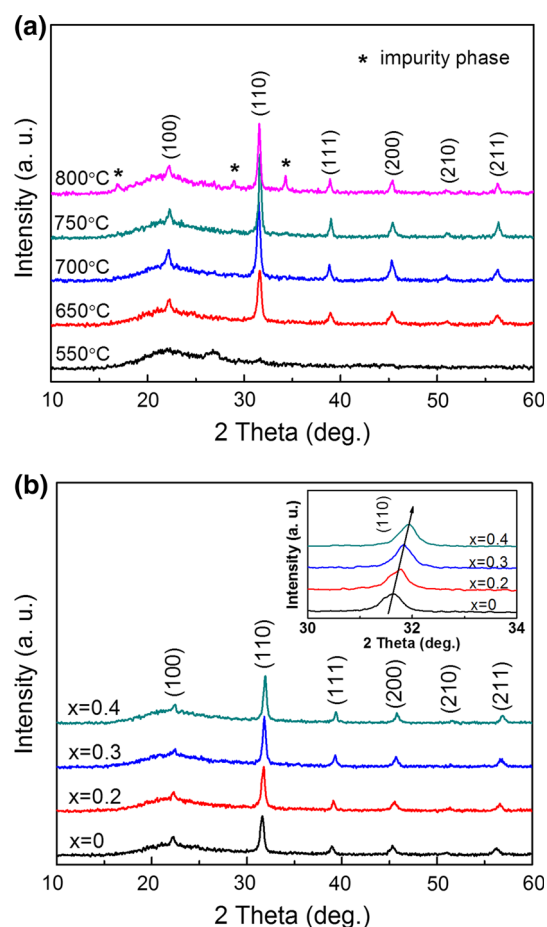


Fig. 1 XRD patterns of **a** $\text{BaTiO}_3:\text{Eu}$ thin films annealed at different temperatures, **b** $\text{Ba}_{1-x}\text{Sr}_x\text{TiO}_3:\text{Eu}$ thin films annealed at 650 °C. The inset shows the magnified (110) diffraction peaks between 30° and 34° (Color figure online)

around 22° came from the fused silica substrate. When the annealing temperature reached 650 °C, the BTE thin films were well crystallized with typical perovskite structure. With increasing annealing temperature, the values of full width at half maximum (FWHM) as well as the intensities of the diffraction peaks were enhanced, suggesting a better crystallinity of the thin films. When the annealing temperature was further increased to 800 °C, extra diffraction peaks marked with asterisk symbols were observed, indicating the formation of impurity phases.

Figure 1b shows the XRD patterns of the $\text{Ba}_{1-x}\text{Sr}_x\text{TiO}_3:\text{Eu}$ (BSTE, $x = 0, 0.2, 0.3,$ and 0.4) thin films deposited on fused silica substrates annealed at 650 °C. All the peaks can be indexed as a single phase of perovskite. The inset shows the magnified (110) diffraction peaks between 30° and 34°. As the Sr^{2+} concentration increased, the diffraction peaks shifted towards higher diffraction angles as a result of contraction in unit-cell volume because the substituted Sr^{2+} ions were smaller in ionic radius than the host Ba^{2+} ions. Besides, the diffraction peaks became

stronger and sharper with increasing Sr^{2+} content. The FWHM values of the (110) diffraction peaks were 0.413, 0.404, 0.384, and 0.347, respectively, for the BSTE thin films with Sr content x values of 0, 0.2, 0.3, and 0.4. With increasing Sr content x , the FWHM values decreased, indicating better crystallinity and larger average crystallite size.

Figure 2 shows the AFM images of the $\text{Ba}_{1-x}\text{Sr}_x\text{TiO}_3:\text{Eu}$ (BSTE, $x = 0, 0.2, 0.3,$ and 0.4) thin films deposited on fused silica substrates annealed at $650\text{ }^\circ\text{C}$. The AFM images were obtained with an area of $1\text{ }\mu\text{m} \times 1\text{ }\mu\text{m}$. The average grain size and surface roughness were analyzed. As can be seen, the thin films were dense with smooth surface and uniform grain size. The root mean square roughness (RMS) of all samples was $\sim 5\text{ nm}$ and the average grain size was $50\text{--}60\text{ nm}$. With the increase of Sr content, the average grain size of the films increased slightly, which can be attributed to the better crystallinity.

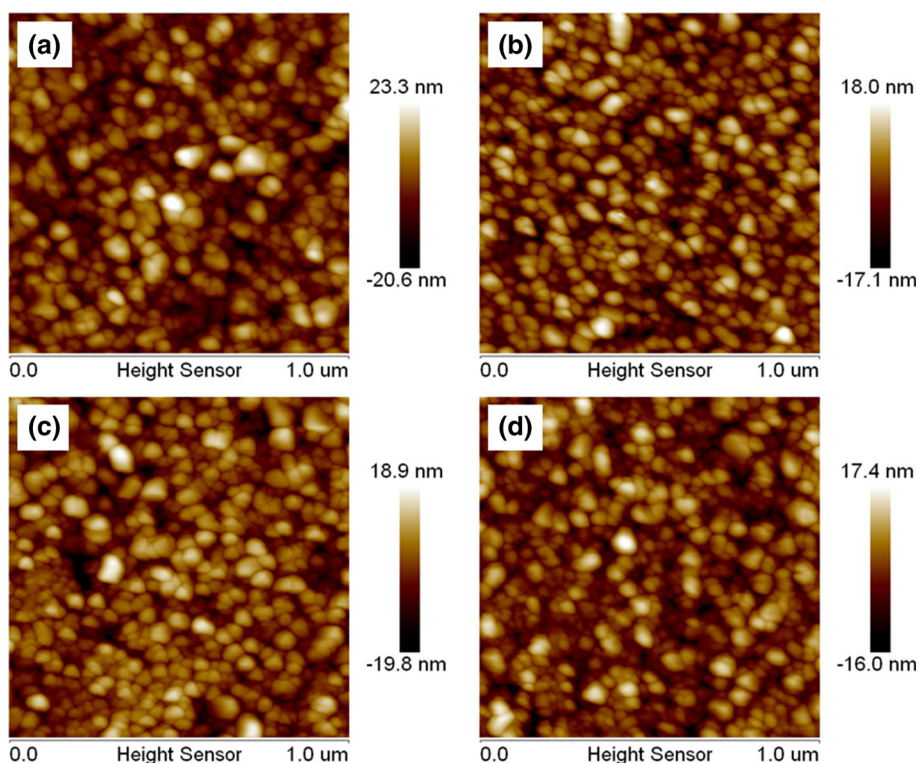
Figure 3a shows the optical transmission spectra in the wavelength range $200\text{--}800\text{ nm}$ of the $\text{Ba}_{1-x}\text{Sr}_x\text{TiO}_3:\text{Eu}$ (BSTE, $x = 0, 0.2, 0.3,$ and 0.4) thin films deposited on fused silica substrates. The films were highly transparent for wavelength longer than about 400 nm and the transmittance dropped off drastically in the short wavelength range. The average transmission in the visible range was about 85% with strong interference oscillations in the long wavelength region, which came from the interference due

to reflection from the top surface of the film and the interface between the film and substrate [20].

The optical band-gap E_g for the thin films can be calculated by considering a direct transition between the valence and conduction bands. In this case, the absorption coefficient α is related to phonon energy as $(\alpha h\nu)^2 = C(h\nu - E_g)$, where $h\nu$ is the incident phonon energy and C is a constant [21]. α is obtained from the absorption spectra, which is shown in the inset of Fig. 3a. The $(\alpha h\nu)^2$ versus $h\nu$ curves for the $\text{Ba}_{1-x}\text{Sr}_x\text{TiO}_3:\text{Eu}$ (BSTE, $x = 0, 0.2, 0.3,$ and 0.4) thin films are shown in Fig. 3b. In a certain range $(\alpha h\nu)^2$ varied linearly with $h\nu$. The band-gap E_g of the films can be determined by extrapolating the linear portion of the curves relating $(\alpha h\nu)^2$ versus $h\nu$ to $(\alpha h\nu)^2 = 0$. The band-gap values thus obtained were $3.71, 3.68, 3.64,$ and 3.63 eV , respectively, for the BSTE thin films with x values of $0, 0.2, 0.3,$ and 0.4 . With the increase of Sr content x , the band-gap of the films shifted to a lower energy. Some researchers have reported that the shift of optical band-gap energy was due to quantum-size effect and existence of some amorphous phases [21, 22]. For our BSTE thin films, the shift can be attributed to a better crystallinity with increasing Sr content, which had an influence on the band-gap energy.

Figure 4a shows the excitation spectra and emission spectra of the $\text{Ba}_{1-x}\text{Sr}_x\text{TiO}_3:\text{Eu}$ (BSTE, $x = 0, 0.2, 0.3,$ and 0.4) thin films monitored at 618 and 395 nm , respectively. The excitation spectra monitored at 618 nm exhibit

Fig. 2 AFM images of $\text{Ba}_{1-x}\text{Sr}_x\text{TiO}_3:\text{Eu}$ thin films annealed at $650\text{ }^\circ\text{C}$ with **a** $x = 0$, **b** $x = 0.2$, **c** $x = 0.3$, and **d** $x = 0.4$



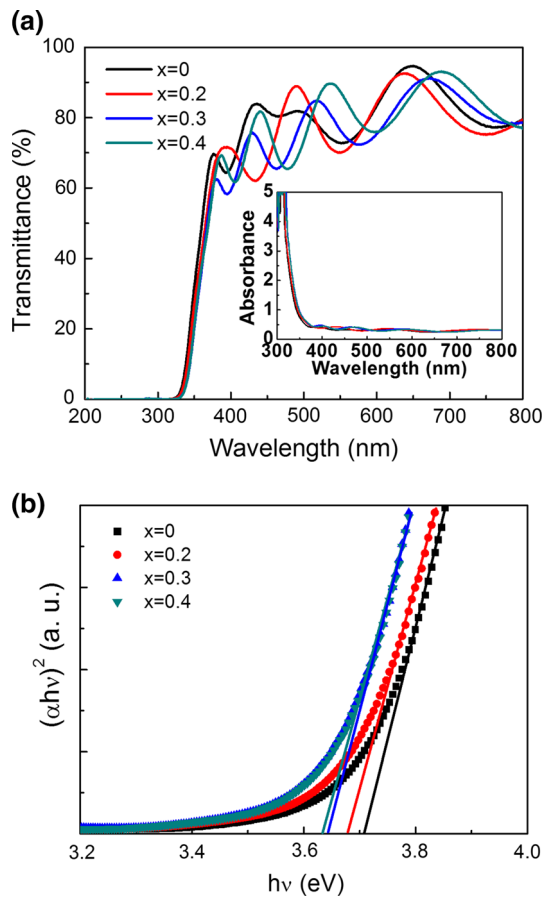


Fig. 3 **a** Optical transmission spectra of $\text{Ba}_{1-x}\text{Sr}_x\text{TiO}_3\text{:Eu}$ thin films annealed at 650 °C. The inset shows the absorption spectra. **b** Plots of $(\alpha h\nu)^2$ versus $h\nu$ (Color figure online)

the peaks corresponding to excitation of the ${}^7\text{F}_0$ ground state to the ${}^5\text{D}_4$ (362 nm), ${}^5\text{L}_7$ (382 nm), ${}^5\text{L}_6$ (395 nm), ${}^5\text{D}_3$ (415 nm) and ${}^5\text{D}_2$ (465 nm) states. The most intense excitation peak, located at 395 nm, corresponds to the ${}^7\text{F}_0 \rightarrow {}^5\text{L}_6$ transition of Eu^{3+} ions. The emission spectra excited with 395 nm wavelength consist of the peaks arising from the relaxation of the ${}^5\text{D}_0$ excited state to the ${}^7\text{F}_0$ (580 nm), ${}^7\text{F}_1$ (594 nm), ${}^7\text{F}_2$ (618 nm), ${}^7\text{F}_3$ (655 nm), and ${}^7\text{F}_4$ (704 nm) states. The two prominent emission peaks centered at 594 nm and 618 nm are assigned to the ${}^5\text{D}_0 \rightarrow {}^7\text{F}_1$ transition and the ${}^5\text{D}_0 \rightarrow {}^7\text{F}_2$ transition of Eu^{3+} ions, respectively.

It is well known that the relative intensities of the $4f \rightarrow 4f$ transitions of the Eu^{3+} ions are strongly influenced by the symmetry of the local atomic environment. Especially the analysis of the spectral features of ${}^5\text{D}_0 \rightarrow {}^7\text{F}_{1,2}$ transitions is of great importance to study the local environment of Eu^{3+} ions. ${}^5\text{D}_0 \rightarrow {}^7\text{F}_2$ is known as an electric dipole transition, which occurs when Eu^{3+} ions occupy the non-centrosymmetry sites, whereas ${}^5\text{D}_0 \rightarrow {}^7\text{F}_1$ is a magnetic dipole transition, which is allowed when Eu^{3+} ions locate at the site of inversion symmetry [3, 23]. The ratio of the integrated

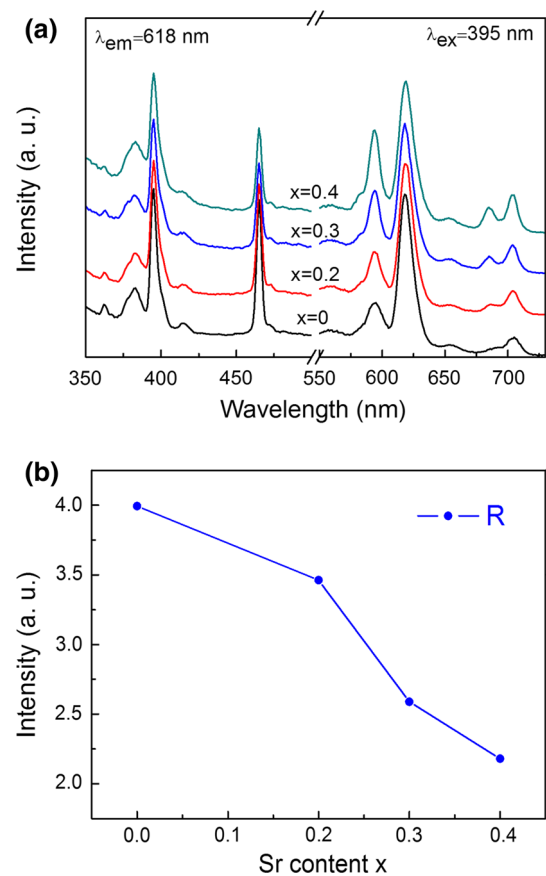


Fig. 4 **a** Excitation and emission spectra of $\text{Ba}_{1-x}\text{Sr}_x\text{TiO}_3\text{:Eu}$ thin films annealed at 650 °C. **b** $R = I({}^5\text{D}_0 \rightarrow {}^7\text{F}_2)/I({}^5\text{D}_0 \rightarrow {}^7\text{F}_1)$ versus Sr content x for the thin films (Color figure online)

emission intensity of the ${}^5\text{D}_0 \rightarrow {}^7\text{F}_2$ (red) to that of the ${}^5\text{D}_0 \rightarrow {}^7\text{F}_1$ (orange), defined as the asymmetry factor R , can be used to investigate the symmetry of the sites occupied by Eu^{3+} ions [8, 24]. The larger the ratio is, the more asymmetric sites the Eu^{3+} ions occupy.

In the ABO_3 perovskite structure, one B-site ion is coordinated by six O^{2-} ions, which makes up a BO_6 octahedron. A-site ions are located on the interstitial space of the BO_6 skeleton and each A-site ion is coordinated by twelve O^{2-} ions [19]. For our BSTe thin films, Ba^{2+} (1.35 Å) and Sr^{2+} (1.18 Å) ions locate at A-sites and Ti^{4+} (0.61 Å) ions locate at B-sites. Mid-sized Eu^{3+} (0.95 Å) ions can be doped at the A-site or B-site as well as both sites simultaneously. When doped at a low concentration, Eu^{3+} ions preferentially substitute for A-site ions [9, 25].

Note that in the emission spectra shown in Fig. 4a, the ${}^5\text{D}_0 \rightarrow {}^7\text{F}_2$ transition near 618 nm is dominant compared to the ${}^5\text{D}_0 \rightarrow {}^7\text{F}_1$ transition near 594 nm, suggesting the environment of Eu^{3+} sites is heavily distorted and lacks inversion symmetry. This is because substituted Eu^{3+} ions are smaller than the host A-site ions, resulting in a lattice contraction and structural distortion. As the Sr content x

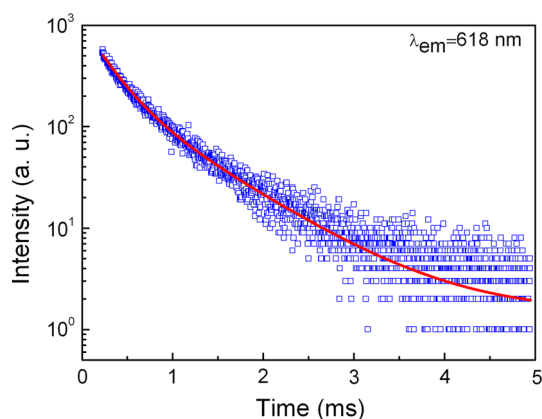


Fig. 5 Emission decay curve for the $\text{Ba}_{1-x}\text{Sr}_x\text{TiO}_3:\text{Eu}$ ($x = 0.3$) thin film monitored at 618 nm. The blue scattering dots are experimental data and the red solid line is fitting result (Color figure online)

increased, no remarkable change was observed in the intensity of ${}^5\text{D}_0 \rightarrow {}^7\text{F}_2$ transition, whereas there was a significant intensity enhancement of the ${}^5\text{D}_0 \rightarrow {}^7\text{F}_1$ transition. The films displayed red-to-orange ratios of 3.99, 3.46, 2.59, and 2.18 for Sr content x values of 0, 0.2, 0.3, and 0.4, respectively. The dependence of asymmetry factor R on different Sr content x was shown in Fig. 4b. The decreasing R with an increasing x indicated that the Eu^{3+} ions occupied more symmetric sites upon increasing Sr content. The result can be explained as follows: when Sr content increased, the average ionic radius of A-site reduced, resulting in a smaller difference of ionic radii between substituted Eu^{3+} ions and host A-site ions. Thus the substitution of Eu^{3+} ions caused less localized contraction of the unit cell and resulted in less lattice distortion, which was believed to be responsible for the decrease of R .

The luminescent decay behaviors of the BSTE thin films were also investigated under the excitation of 395 nm. Figure 5 shows the decay curve for the $\text{Ba}_{1-x}\text{Sr}_x\text{TiO}_3:\text{Eu}$ (BSTE, $x = 0.3$) thin film monitored at 618 nm. The decay curve can be well fitted with second order exponential decay equation $I = I_1 \exp(-t/\tau_1) + I_2 \exp(-t/\tau_2)$, where I_1 and I_2 are intensities at two different interval times and corresponding decay times are τ_1 and τ_2 . The τ_1 and τ_2 values were found to be 0.26 ms ($I_1 = 36\% I$) and 0.78 ms ($I_2 = 64\% I$), respectively. The average lifetime τ was calculated to be 0.7 ms by using the equation $\tau = (I_1 \tau_1^2 + I_2 \tau_2^2) / (I_1 \tau_1 + I_2 \tau_2)$. It has been reported that Eu^{3+} , Bi^{3+} co-doped $(\text{Ca},\text{Sr})(\text{Mo},\text{W})\text{O}_4$ red-emitting phosphors had an similar average lifetime [26].

4 Conclusions

Eu-doped $\text{Ba}_{1-x}\text{Sr}_x\text{TiO}_3$ ($x = 0, 0.2, 0.3,$ and 0.4) thin films have been fabricated on fused silica substrates by a

chemical solution deposition method. The films were well crystallized with a pure perovskite structure in the annealing temperature range 650–750 °C. The optical transmission spectra showed that the films were highly transparent in the visible wavelength region. The band-gap energies of the films were also investigated. The more the Sr content in the thin films, the narrower the energy gap of the thin films. Photoluminescence spectra showed two prominent transitions of Eu^{3+} ions at 594 nm (${}^5\text{D}_0 \rightarrow {}^7\text{F}_1$) and 618 nm (${}^5\text{D}_0 \rightarrow {}^7\text{F}_2$) upon excitation at 395 nm (${}^7\text{F}_0 \rightarrow {}^5\text{L}_6$). The observed changes of luminescence spectra by the decrease of the intensity ratio R , defined as the ratio of the integrated emission intensity of the ${}^5\text{D}_0 \rightarrow {}^7\text{F}_2$ to that of the ${}^5\text{D}_0 \rightarrow {}^7\text{F}_1$, were associated with the increase of the inversion symmetry of Eu^{3+} sites when Sr content increased. Lifetime study of photoluminescence indicated that the average lifetime of the thin films was ~ 0.7 ms.

Acknowledgments The authors gratefully acknowledge financial support from Natural Science Foundation of China (No. 51172289), National Basic Research Program (973 Program) of China (No. 2012CB619302), and the Specialized Research Fund for the Doctoral Program of Higher Education of China (No. 20110171130004).

References

1. R. Reshmi, M.K. Jayaraj, K. Jithesh, M.T. Sebastian, J. Electrochem. Soc. **157**, H783–H786 (2010)
2. C. Shen, Q. Liu, Q.F. Liu, Mater. Sci. Eng. B **111**, 31–35 (2004)
3. Q. Yang, L. Fang, F. Zheng, M. Shen, Mater. Chem. Phys. **118**, 484–489 (2009)
4. S. Saha, S.B. Krupanidhi, Appl. Phys. Lett. **79**, 111–113 (2001)
5. W. Strek, D. Hreniak, G. Boulon, Y. Guyot, R. Pązik, Opt. Mater. **24**, 15–22 (2003)
6. C.L. Freeman, J.A. Dawson, J.H. Harding, L.B. Ben, D.C. Sinclair, Adv. Funct. Mater. **23**, 491–495 (2013)
7. T. Montini, A. Speghini, L. De Rogatis, B. Lorenzut, M. Bettinelli, M. Graziani, P. Fornasiero, J. Am. Chem. Soc. **131**, 13155–13160 (2009)
8. C. Zhu, S. Chaussedent, S. Liu, Y. Zhang, A. Monteil, N. Gaurier, Y. Yue, J. Alloys Compd. **555**, 232–236 (2013)
9. F.A. Rabuffetti, S.P. Culver, J.S. Lee, R.L. Brutchey, Nanoscale **6**, 2909–2914 (2014)
10. F.A. Rabuffetti, J.S. Lee, R.L. Brutchey, Adv. Mater. **24**, 1434–1438 (2012)
11. H.-F. Cheng, J. Appl. Phys. **79**, 7965–7971 (1996)
12. T. Zhang, H. Gu, J. Liu, Microelectron. Eng. **66**, 860–864 (2003)
13. P.K. Sharma, G.L. Messing, D.K. Agrawal, Thin Solid Films **491**, 204–211 (2005)
14. D.Y. Wang, J. Wang, H.L.W. Chan, C.L. Choy, J. Appl. Phys. **101**, 043515 (2007)
15. S. Kongtaweelert, D.C. Sinclair, S. Panichphant, Curr. Appl. Phys. **6**, 474–477 (2006)
16. C.B. Samantaray, M.L.N. Goswami, D. Bhattacharya, S.K. Ray, H.N. Acharya, Mater. Lett. **58**, 2299–2301 (2004)
17. W. Zhang, H. Wang, J. Chen, W. Zhang, X. Xiong, J. Zhang, J. Lumin. **128**, 1359–1362 (2008)

18. Y. Gim, T. Hudson, Y. Fan, C. Kwon, A.T. Findikoglu, B.J. Gibbons, B.H. Park, Q.X. Jia, *Appl. Phys. Lett.* **77**, 1200–1202 (2000)
19. D.-Y. Lu, T. Ogata, H. Unuma, X.-C. Li, N.-N. Li, X.-Y. Sun, *Solid State Ion.* **201**, 6–10 (2011)
20. H. Guo, L. Liu, Z. Chen, S. Ding, H. Lu, K.-J. Jin, Y. Zhou, B. Cheng, *Europhys. Lett.* **73**, 110–115 (2006)
21. D. Bao, X. Yao, N. Wakiya, K. Shinozaki, N. Mizutani, *Appl. Phys. Lett.* **79**, 3767–3769 (2001)
22. H. Gu, D. Bao, S. Wang, D. Gao, A. Kuang, X. Li, *Thin Solid Films* **283**, 81–83 (1996)
23. H. Zhang, X. Fu, S. Niu, Q. Xin, *J. Alloys. Compd.* **459**, 103–106 (2008)
24. J. Fu, J. Zhao, T. Sa, N. Qin, D. Bao, *Appl. Surf. Sci.* **286**, 1–6 (2013)
25. C. Jiang, L. Fang, M. Shen, F. Zheng, X. Wu, *Appl. Phys. Lett.* **94**, 071110-1–071110-3 (2009)
26. H.D. Xie, F. Li, H.H. Xi, R. Tian, X.C. Wang, *J. Mater. Sci. Mater. Electron.* **26**, 23–31 (2015)